MoCaE: Mixture of Calibrated Experts Significantly Improves Object Detection

Kemal Oksuz, Selim Kuzucu, Tom Joy, Puneet K. Dokania
Five AI Ltd., United Kingdom
{kemal.oksuz, selim.kuzucu, tom.joy, puneet.dokania}@five.ai

Abstract

We propose an extremely simple and highly effective approach to faithfully combine different object detectors to obtain a Mixture of Experts (MoE) that has a superior accuracy to the individual experts in the mixture. We find that naïvely combining these experts in a similar way to the well-known Deep Ensembles (DEs), does not result in an effective MoE. We identify the incompatibility between the confidence score distribution of different detectors to be the primary reason for such failure cases. Therefore, to construct the MoE, our proposal is to first calibrate each individual detector against a target calibration function. Then, filter and refine all the predictions from different detectors in the mixture. We term this approach as Mixture of Calibrated Experts (MoCaE) and demonstrate its effectiveness through extensive experiments on object detection, instance segmentation and rotated object detection tasks. Specifically, MoCaE improves (i) three strong object detectors on COCO test-dev by 2.4 *AP by reaching* 59.0 *AP; (ii) instance segmentation methods on the challenging long-tailed LVIS dataset by* 2.3 *AP; and (iii) all existing rotated object detectors by reaching* 82.62 AP_{50} *on DOTA dataset, establishing a new state-of-the-art (SOTA). Code will be made public.*

1. Introduction

Several real-world applications such as autonomous driving [4, 18, 58], medical imaging [65], surveillance [63] or auto-labelling [28, 33] require accurate object detectors. As a result, various aspects of object detectors, including data augmentation [10, 15, 16, 72], exploiting unlabelled additional data [70, 73], model design [22, 25, 39, 45, 68] and loss functions [9, 37, 38, 42, 44, 51, 62], have been extensively studied. Surprisingly, ensembling detectors either in the form of a DE by using the same model with different initializations or as an MoE by combining different type of models has received very little attention [7, 36], despite their success in the classification literature [34]. In this paper, we focus on this important gap in the literature, and propose a method that is simple, principled and effective at obtaining an MoE in object detection.

Mechanically, a DE requires combining predictions from multiple models; mathematically this approximates the *posterior predictive* through Monte-Carlo sampling of the parameter space. MoE however performs this sampling on the distribution of model functions, thereby reducing the bias and as such one would expect an MoE to have superior performance over its DE counterpart. However, we observe that this is in fact not the case, as the confidence scores for each detection are generally incompatible across detectors, due to different training procedures, post-processing operations or architectures.

In order for an MoE to faithfully combine the detections so that the detectors complement each other, the underlying predictive distributions for each posterior estimate must be compatible. To achieve this, we observe that calibrating their confidence scores using the same underlying target function is crucial. This brings them to a common ground where the confidence scores of different detectors are now compatible.

To illustrate this, Fig. 1(a) displays the confidence score distributions of RS R-CNN [52], a two-stage detector optimized by a ranking-based loss; ATSS [69], a one-stage detector obtaining the final confidence as the product of classification confidence and centerness [59]; and PAA [27] with the same architecture as ATSS but combining Intersection-over-Union (IoU) and classification confidence using geometric mean to obtain the final confidence. Due to these idiosyncrasies, the confidence score distributions of these detectors differ completely as shown in Fig. 1(a). For example, RS R-CNN has significantly higher confidence than ATSS on the same subset of images. Thereby rendering utilising an MoE in a similar way a practitioner would use a DE infeasible, as the detector with the highest confidence will dominate the MoE, regardless of its accuracy.

In this paper, we propose MoCaE as a simple and effective method to address this problem and enable accurate MoEs for object detectors. At a high level, MoCaE combines a calibration method, such as Isotonic Regression (IR) [66], with a post-hoc approach for aggregation such as Non-Maximum Suppression (NMS) or its variants [1, 27]. Consequently, MoCaE now makes the confidence scores

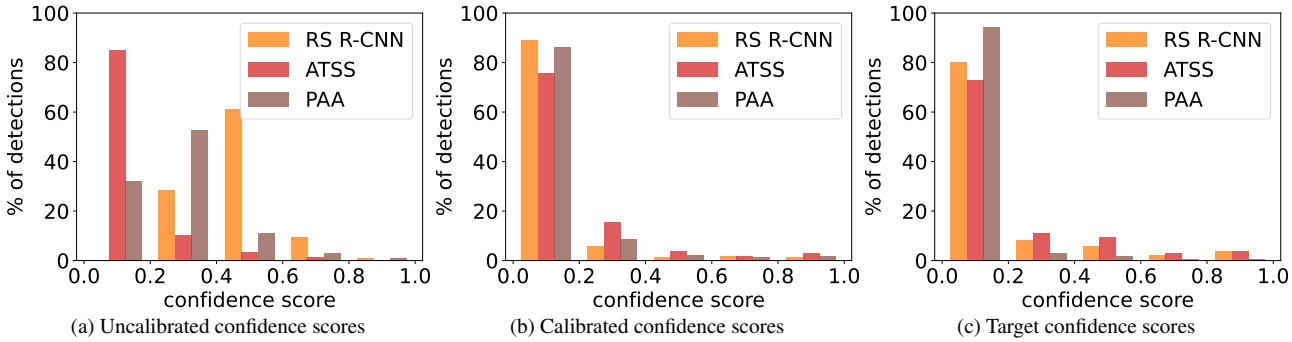

(a) Uncalibrated confidence scores (b) Calibrated confidence scores (c) Target confidence scores

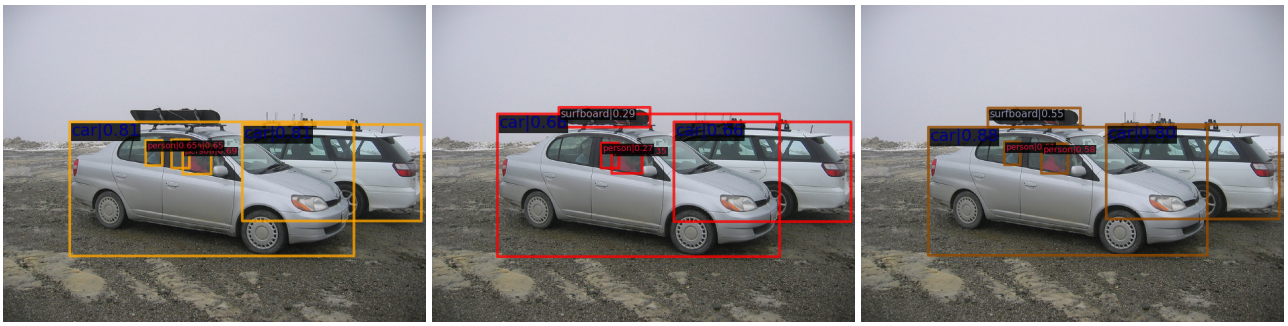

(d) Expert 1: RS R-CNN (e) Expert 2: ATSS (f) Expert 3: PAA

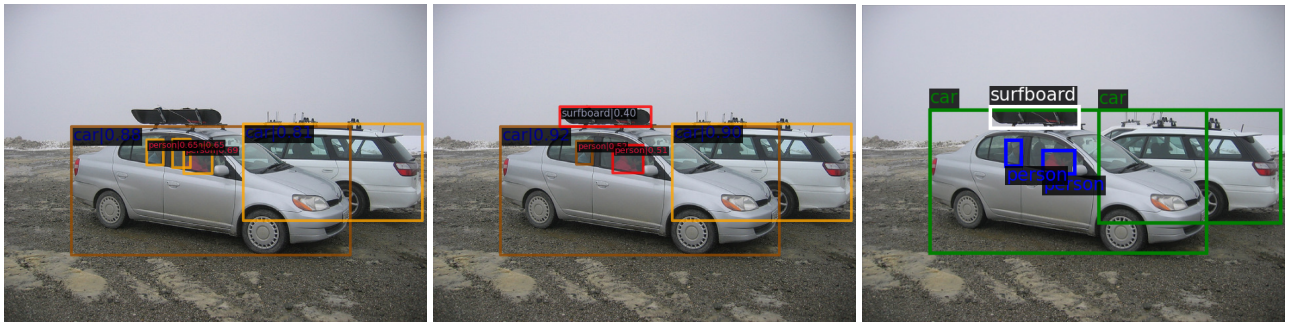

(g) Mixture of Uncalibrated Experts (h) Mixture of Calibrated Experts (i) Ground Truth Objects

Figure 1. The detections and histograms are color-coded. orange: RS R-CNN, red: ATSS, brown: PAA. **(a-c)** The distribution of the uncalibrated, calibrated and the target confidence on half of the COCO [43] val set with 2.5K images. MoCaE uses IoU of the detection as the target confidence. The detectors exhibit different distributions unless they are calibrated. **(d-f)** Outputs of the detectors on an example image. RS R-CNN misses the "surfboard", ATSS misses a "person", PAA has a notable localisation error for the "person" in front seat. **(g-i)** The detections from MoE of uncalibrated detectors; MoE of calibrated detectors; and the ground truth. (g) is dominated by the most confident RS R-CNN and misses the "surfboard". After calibration in (h), all objects are detected accurately by mitigating the errors of single detectors.

of the aforementioned detectors comparable as shown in Fig. 1(b,c). Fig. 1(d-i) presents the benefit of MoCaE on an example in which we combine the same three detectors, yielding the detections in Fig. 1(d-g). Note that the MoE of uncalibrated detectors in Fig. 1(g) is dominated by the most confident RS R-CNN with only one detection contribution from PAA and none from ATSS. As a result, this MoE misses the "surfboard" and has a "person" as a false-positive (FP). After calibration, all detectors contribute to the MoE, which finally detects all objects accurately in Fig. 1(h). In this example, the resulting MoE is more accurate than the single detectors. This is because, RS R-CNN (Fig. 1(d)) fails to detect the surfboard, ATSS (Fig. 1(e)) misses the person in the rear seat and PAA (Fig. 1(f)) has a notable localisation error for the person in the front seat. Although this example was chosen for brevity, we demonstrate that this pathology is present across many samples in the datasets. Overall, our contributions can be summarized as follows:

1. We show that the incompatibility of confidence scores across different detectors is the main challenge to obtain accurate MoEs for object detection. To remedy this, we propose MoCaE as an extremely simple, highly effective and principled method that combines post-hoc calibrators with aggregation approaches such as NMS or its variants.

2. We show that MoCaE performs much better than DEs even with fewer detectors in the mixture compared to that of in DEs. As an example, combining only ATSS and PAA using MoCaE on par with DEs with 5 components from

either of these detectors, and using RS R-CNN as the third component outperforms these DEs.

3. MoCAE yields significant gain over the single models on different real world challenging detection tasks: (i) For object detection, our MoCAE combining three strong detectors reaches 59.0 AP on COCO test-dev [43] **with a gain of** 2.4 **AP** compared to the best single model; (ii) for instance segmentation, MoCAE improves Mask R-CNN with ResNeXt-101 by 2.3 AP on the long-tailed LVIS dataset [20] *with more than 1K object categories*; (iii) for rotated object detection, we reach 82.62 AP on DOTA dataset [63] **as a new SOTA**.

2. Background and Notations

Object Detection Given that the set of M objects in an image X is represented by $\{b_i, c_i\}^M$ where $b_i \in \mathbb{R}^4$ is a bounding box and $c_i \in \{1, \dots, K\}$ its class; the goal of an object detector is to predict the bounding boxes and the class labels for the objects in X, $f(X) = \{\hat{c}_i, \hat{b}_i, \hat{p}_i\}^N$, where $\hat{c}_i, \hat{b}_i, \hat{p}_i$ represent the class, bounding box and confidence score of the ith detection respectively and N is the number of predictions. In general, the detections are obtained in two steps, $f(X) = (h \circ g)(X)$ [6, 44, 56, 57]: where $g(X) = \{\hat{b}_i^{raw}, \hat{p}_i^{raw}\}^{N^{raw}}$ is a deep neural network predicting raw detections with bounding boxes $\hat{b}_i^{raw}$ and predicted class distribution $\hat{p}_i^{raw}$. Then, in the second step, $h(\cdot)$ applies post-processing to raw-detections and the final detections are obtained. In general, $h(\cdot)$ consists of discarding the detections predicted as background; NMS to remove the duplicates; and keeping useful detections, normally achieved via top-k survival, where typically $k = 100$ for COCO.

Calibration of Object Detectors As extensively studied for classification, calibration refers to the alignment of accuracy and confidence of a model [11, 19, 30, 47, 49, 61]. Specifically, a classifier is said to be *calibrated* if it yields an accuracy of p on its predictions with a confidence of p for all $p \in [0, 1]$. Earlier definitions for the calibration of detectors [31, 48] extend this definition with an objective to align the confidence of a detector with its precision,

$$\mathbb{P}(\hat{c}_i = c_i | \hat{p}_i) = \hat{p}_i, \forall \hat{p}_i \in [0, 1], \tag{1}$$

where $\mathbb{P}(\hat{c}_i = c_i | \hat{p}_i)$ denotes the precision as the ratio of correctly classified predictions among all detections. Extending from this definition, [54] takes into account that object detection is a joint task of classification and localisation. Thereby defining the accuracy as the product of precision and average IoU of true-positives (TPs), calibration of object detectors requires the following to be true

$$\mathbb{P}(\hat{c}_i = c_i | \hat{p}_i) \mathbb{E}_{\hat{b}_i \in B_i(\hat{p}_i)}[\mathrm{IoU}(\hat{b}_i, b_{\psi(i)})] = \hat{p}_i, \forall \hat{p}_i \in [0, 1], \tag{2}$$

where $B_i(\hat{p}_i)$ is the set of TPs with the confidence of $\hat{p}_i$ and $b_{\psi(i)}$ is the object that $\hat{b}_i$ matches with. Then, Localisation-aware Expected Calibration Error (LAECE) is obtained by discretizing the confidence score space into J bins for each class. Specifically for class c, denoting the set of detections by $\hat{\mathcal{D}}^c$ and those in the jth bin by $\hat{\mathcal{D}}_j^c$ as well as the average confidence, precision and average IoU of $\hat{\mathcal{D}}_j^c$ by $\bar{p}_j^c$, $\mathrm{precision}^c(j)$ and $\bar{\mathrm{IoU}}^c(j)$ respectively, LAECE for class c is defined as

$$\mathrm{LaECE}^c = \sum_{j=1}^{J} \frac{|\hat{\mathcal{D}}_j^c|}{|\hat{\mathcal{D}}^c|} \left| \bar{p}_j^c - \mathrm{precision}^c(j) \times \bar{\mathrm{IoU}}^c(j) \right|. \tag{3}$$

Finally, the detector LAECE is the average of LaECE^cs over classes in the dataset, measuring the calibration error for a detector as a lower-better measure.

3. Enabling Accurate Mixture of Experts via Calibration

It is interesting to ask why the confidence score distributions vary significantly, despite the fact that the detectors perform similarly. Among different factors causing this incompatibility, one major factor is related to the architectures employed. For example, some recent detectors employ an additional auxiliary head to predict localisation confidence [24, 25, 27, 59, 69]. Then the final confidence is taken as an increasing function of classification and localisation confidences. Consequently, the auxiliary head choice such as centerness [59, 69] or IoU [25, 27] as well as the aggregation function such as multiplication [59, 69] or geometric mean [27] provides significant variation in the confidence scores. Architectural difference can also manifest itself in the type of the detector, which can be fully convolutional one-stage [59, 69], two-stage [5, 56], bottom-up [14, 35] as well as transformer-based detectors [6, 71]. Arguably, another factor causing the confidence incompatibility across the detectors is the used classifier, which commonly vary between a softmax [2, 6, 12, 56] or sigmoid classifiers for each class [27, 44, 69, 71]. Besides, following from the classifiers, different backbones [55], loss functions [47] and the training length [47, 54] affect the confidence of the model.

The Issue with Vanilla MoE As the confidence scores of different detectors are incompatible, as we will show here, combining them naïvely does not yield a strong MoE. The most confident detector dominates the MoE regardless of its accuracy. To show this, similar to [7], we construct a "Vanilla MoE" which aggregates the final predictions from RS R-CNN [52], ATSS [69] and PAA [27] using NMS. Fig. 2(a) shows that Vanilla MoE is dominated by the most confident RS R-CNN (following the setting in Fig. 1(a)) with a small contribution from less confident PAA and almost no detections from the least confident ATSS. As a result, while one would expect an MoE to detect more objects than individual detectors and obtain a better recall, Tab. 1(bottom) shows the opposite; *Vanilla MoE yields a lower Average Recall (AR) compared to ATSS and PAA*. The aforementioned issue

Calibration	RS-RCNN	ATSS	PAA
✗	36.45	5.01	11.23
✓	**3.15**	**4.51**	**1.62**

Method	R@0.50	R@0.75	AR
RS R-CNN	83.2	62.7	58.3
ATSS	83.1	65.9	60.8
PAA	83.4	65.8	61.1
Vanilla MoE	83.6	64.1	59.7
MoE after cal.	**85.1**	**67.7**	**62.3**

Table 1. **(Top)** LAECE of detectors before and after calibration (cal.). **(Bottom)** Recall@IoU (R@IoU) and AR using 100 detections.

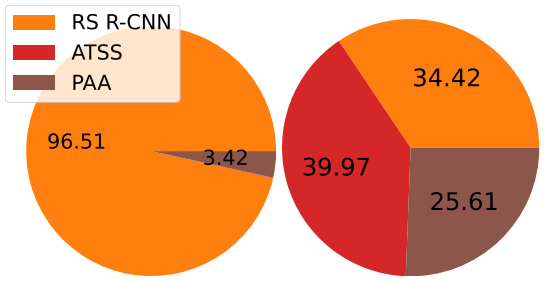

(a) Vanilla MoE (b) MoE after cal.

Figure 2. Piecharts representing the % of detections obtained from a certain detector in the final detection set of MoEs. **(a)** MoE of uncalibrated detectors and **(b)** MoE of calibrated detectors.

clearly indicates that naïvely obtaining MoE will normally be biased and lead to an ineffective mixture.

We have now highlighted that a fundamental issue with constructing an MoE, is that a situation can often arise when one of the detector dominates the predictions. However, this is not necessarily a deficiency, as one would expect an accurate detector to dominate the predictions when combined with inaccurate ones. The question naturally arises as to what the appropriate contribution from each detector is in the final output. Conceptually, we want the MoE to combine predictions based on their performance, which can be inferred through the confidence estimates provided at test time. However, these confidence estimates are typically unaligned with the models performance, a pathology known as miscalibration. Consequently, to appropriately combine detectors, we first calibrate them individually, enabling reliable contributions from each detector. We report LAECE in Tab. 1 (top) where we see that RS-RCNN has the largest LAECE, indicating that its contribution to the Vanilla MoE is not based on its perfomance.

3.1. Introducing MoCaE

Motivated from this example, we seek to address this issue and obtain MoEs with appropriate contributions form the individual detectors. To do this, we introduce MoCaE that (i) solves this incompatibility issue via calibrating the confidence scores, and (ii) filters out the duplicates from different detectors and refines the detections to have a higher IoU.

3.1.1 Appropriate Choice of Calibration Function

Having identified the issue with the Vanilla MoE, the question naturally arises as to how we calibrate the single detectors to address this deficiency. As opposed to the standard classification task, object detection jointly solves both classification and regression tasks; and also involves various post-processing steps that can influence the accuracy of the detector. Therefore, it is not straightforward as to what objective the final calibrator should have and at which stage of the pipeline it should be applied. A natural choice would be to calibrate the scores such that it helps the most crucial aggregation stage (e.g., NMS). This stage does not require training and practically has significant impact on the performance of a detector.

For simplicity, let's consider the standard NMS, which groups the detections that have an IoU with the maximum-scoring detection larger than a predefined IoU threshold. Then, within that group, NMS survives the detection with the largest score and removes the remaining detections from the detection set. In such a setting, as also discussed by the recent works [25, 26, 37, 38, 69], the ideal confidence that should be transferred to the NMS is arguably the IoU of the detection with the object. This will help NMS to pick *accurately-localised detections* for the objects detected by multiple detectors. Also, if an object is detected by a single less confident detector, aligning the confidence with IoU implies that the scores of the TPs are to be promoted. Thus, the TPs of a less confident detector will not be dominated by the FPs of more confident ones unlike the case in Fig. 2(a).

Following this intuition, we call a detector calibrated if it yields a confidence that matches the IoU

$$\mathbb{E}_{\hat{b}_i \in B_i(\hat{p}_i)}[\text{IoU}(\hat{b}_i, b_{\psi(i)})] = \hat{p}_i, \forall \hat{p}_i \in [0,1], \qquad (4)$$

where $B_i(\hat{p}_i)$ is the set of detection boxes with the confidence score of $\hat{p}_i$ and $b_{\psi(i)}$ is the ground-truth box that $\hat{b}_i$ has the highest IoU with. Note that this corresponds to using an IoU threshold of 0 to validate TPs. Hence, we use LAECE by setting $\text{precision}^c(j) = 1$ in Eq. (3) throughout the paper.

Choice of calibration method There are multiple post-hoc calibration methods [19, 29], so we investigate Linear Regression (LR) and IR [66] considering the criterion in Eq. (4). We observe that training a Class-agnostic (CA) IR calibrator for each detector on 500 images is sufficient to enable MoEs. Using the same example in Tab. 1 and Fig. 2, we can easily see the positive effect of calibration; LAECE significantly decreases in Tab. 1(top), which enables an MoE with a significantly better AR than the single detectors in Tab. 1(bottom). This is achieved since all detectors con-

tribute to the MoE in a more balanced way after calibration as shown in Fig. 2(b).

Late or Early Calibration Up to now, we discussed calibrating final confidence scores $\hat{p}_i$ similar to [31, 54], which we show as *late calibration* in Fig. 3(a). Besides, we also investigate the effectiveness of *early calibration* by calibrating the raw probabilities $\hat{p}_i^{raw}$ of the detectors as illustrated in Fig. 3(b). While we find both approaches to perform similar in MoEs, we use late calibration as it is more simple owing to the less number of final detections. Still, as the first to investigate early calibration, we demonstrate an additional use-case of early calibration in Sec. 4.3 in which it reduces the sensitivity of the model to the background removal threshold in post-processing in terms of accuracy and efficiency.

3.1.2 Aggregating Calibrated Detections

Given calibrated detections from different detectors (Fig. 3), here we aim to suppress redundant detections targeting the same object and obtain detections with high localisation quality. As aforementioned, NMS is a method that fits for this purpose and, as we observe experimentally, does provide highly competitive results. Alternatively, we construct *Refining NMS* that simply combines Soft NMS [1] with Score Voting [27]. Soft NMS, by design, is less rigid in removing overlapping detections. Instead, it decreases the scores of overlapping boxes that naturally leads to improved recall. Score Voting combines multiple overlapping detections (using their confidences and IoUs with each other) and obtains a refined detection with better localisation. Thus, combining these two approaches leads to a much effective aggregator. Please see App. A for details.

4. Experiments

We now present the benefit of MoCaE on three different tasks, namely: object detection, instance segmentation and rotated object detection. For these tasks, we use a total of 11 different detectors; these architectures are very diverse and include one-stage and two-stage convolutional as well as transformer-based ones. Our experiments clearly demonstrate that calibration is essential to enable accurate MoEs. Specifically, MoCaE improves (i) three strong object detectors on COCO test-dev by 2.4 AP by reaching 59.0 AP; (ii) instance segmentation methods on the challenging long-tailed LVIS dataset by 2.3 AP; and (iii) all existing rotated object detectors by reaching 82.62 AP_{50} on DOTA dataset, establishing a new SOTA. Also, MoCaE yields significant gain compared DEs, even in situation where the number of experts is far fewer than the number of ensemble components.

4.1. MoCaE for Object Detection

Dataset and Performance Measures For object detection we use the common COCO dataset [43]. Similar to [32], we randomly split COCO val set with 5K images into two, and use 2.5K images as COCO *minival* to calibrate the detectors and keep the remaining 2.5K images for testing as COCO *minitest*. We also use COCO *test-dev* with 20K images as a large-scale test set by submitting results to the evaluation server. For evaluation, we mainly use COCO-style Average Precision (AP) and also report (i) AP_{50}, AP_{75} as the APs measured at IoU thresholds 0.50 and 0.75; as well as (ii) AP_S, AP_M and AP_L to present the accuracy on small, medium and large objects.

Used Detectors We obtain MoEs in two different settings using off-the-shelf detectors. First, we employ RS R-CNN, ATSS and PAA with ResNet-50 [21] with FPN [41] backbone. As previously discussed in Sec. 1, they have different characteristics making these detectors non-trivial to combine. Second, to see if our gains generalize to a challenging case, we select the following detectors, which are among the most strong publicly available ones on COCO dataset (please see App.B for details):

- YOLOv7 [60] with a large convolutional backbone following its original setting,
- QueryInst [17] as a transformer-based detector with a Swin-L [45] backbone,
- ATSS with transformer-based dynamic head [13] and again Swin-L backbone.

Calibration is crucial for accurate MoEs We first demonstrate the importance of calibration in obtaining strong MoEs. To do so, we construct three MoEs from pair-wise combinations of RS R-CNN, ATSS and PAA as well as one MoE that combines all three. In order to focus only on calibration, here we use the standard NMS with an IoU threshold of 0.65 as in [60]. Tab. 2 presents the results of MoEs with uncalibrated and calibrated detectors. The striking observation is that *without calibration, the MoEs perform similar to the single models and calibration enables strong MoEs for all four settings.* Specifically, using two calibrated MoEs boosts the performance by $\sim$ 1AP and using three by 1.5AP compared to single models; showing the effectiveness of calibration.

Even with less models, MoCaE performs better than DEs Next we compare MoCaE, Vanilla MoE and DEs. Similar to MoCaE, we obtain DEs by using late calibration with Refining NMS for aggregation. Tab. 3 shows that the DEs perform consistently better than the single models; validating them as strong baselines. The main observation in Tab. 3 is that *combining different types of few detectors into an MoE performs significantly better than DEs.* Specifically, MoCaE with only two detectors, ATSS and PAA, performs on par with all DEs with five components. Also, combining three detectors by MoCaE performs 1 AP better than its

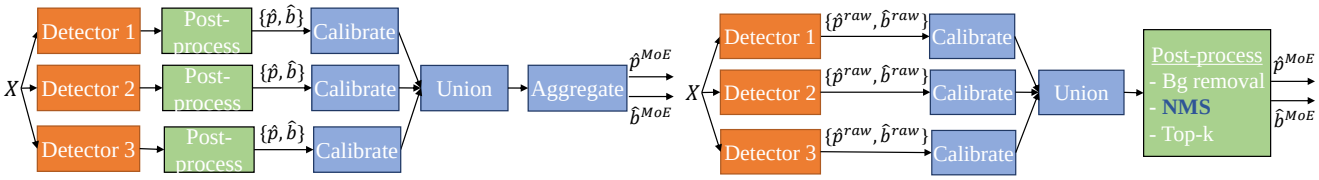

(a) Late Calibration (b) Early Calibration

Figure 3. **(a)** Late calibration. Each detector follows its own pipeline and outputs $\{\hat{p}, \hat{b}\}$ as top-k detections. The confidence scores of final detections $\hat{p}$ are first calibrated, then aggregated via NMS or its variants. We finally get top-k as the detections of MoE $\{\hat{p}^{MoE}, \hat{b}^{MoE}\}$. **(b)** Early calibration. Raw confidence scores $\hat{p}^{raw}$ are calibrated, and the standard post-processing steps handle aggregation in which NMS (in blue) removes the duplicates from multiple detectors.

Table 2. Effect of calibration on MoE performance. All MoEs use Late calibration with standard NMS. While combining uncalibrated detectors do not provide notable gain over the single detectors, calibration is essential for a strong MoE resulting in up to ~ 1.5 AP gain over single detectors.

Model Type	Calibration	Combined Detectors			Object Detection Performance					
		RS R-CNN	ATSS	PAA	AP	AP_{50}	AP_{75}	AP_S	AP_M	AP_L
Single Models	N/A	✓			42.4	62.1	46.2	26.8	46.3	56.9
	N/A		✓		43.1	61.5	47.1	27.8	47.5	54.2
	N/A			✓	43.2	60.8	47.1	27.0	47.0	57.6
Mixtures of Experts	✗	✓	✓		42.4	62.1	46.3	26.8	46.3	**56.9**
	✓	✓	✓		**44.1**	**63.0**	**48.4**	**28.5**	**48.4**	56.8
	✗	✓		✓	43.4	62.5	47.1	27.3	47.3	58.0
	✓	✓		✓	**44.0**	**62.7**	**47.9**	**28.2**	**48.2**	**58.1**
	✗		✓	✓	43.3	60.9	47.2	27.1	47.2	**57.6**
	✓		✓	✓	**44.4**	**62.5**	**48.5**	**29.2**	**48.5**	57.3
	✗	✓	✓	✓	43.4	62.5	47.1	27.3	47.3	58.0
	✓	✓	✓	✓	**44.7**	**63.1**	**48.9**	**29.2**	**49.0**	**58.2**

closest counterpart DE. This is because the same type of detectors make similar errors, which yields less gain once they are combined together. However, different types of detectors complement each other thanks to their diversity. Finally, MoCaE outperforms Vanilla MoE using uncalibrated detectors by 1.1 AP in this stronger setting with Refining NMS as well. Our final model obtains 45.5 AP and outperforms the best single model in all AP variants significantly by between $2-3$ AP. See App.B for the details on DEs.

The gain of MoCaE generalizes to strong object detectors on COCO *test-dev* Until now we used smaller scale (but recently-proposed) detectors. Considering that the performance gain tends to decay in stronger settings, we now investigate how MoCaE performs in such a setting using COCO *test-dev*. As previously described, here we obtain an MoE from YOLOv7, QueryInst and ATSS with dynamic head, which are among the most accurate publicly available detectors. These detectors differ from each other in terms of the pretraining data, backbone or architecture as summarized in Tab. 4. We observe that our MoCaE reaches 59.0 AP with a gain of 2.4 AP gain on this challenging setting as well. Thereby demonstrating the effectiveness of MoCaE on strong detectors.

4.2. MoCaE for Other Detection Tasks

Instance Segmentation We use LVIS [20] as a long-tailed dataset for instance segmentation with more than 1K classes. Following its standard evaluation, we also report the AP on rare (AP_r), common (AP_c) and frequent (AP_f) classes. Similar to COCO, we only reserve 500 images from LVIS val set to calibrate the detectors, and test our models on the remaining 19.5K images of the val set. We combine three recent and diverse off-the-shelf Mask R-CNN variants in a MoE:

- The vanilla Mask R-CNN [22] with ResNeXt-101 [64] backbone, softmax classifier and using Repeat Factor Sampling (RFS) to address the long-tailed nature of LVIS,
- Mask R-CNN with ResNet-50, sigmoid classifier, trained with RS Loss [52] and RFS,
- Mask R-CNN with ResNet-50, softmax classifier, trained with Seesaw Loss[62] but no RFS.

Tab. 5 shows that *while the Vanilla MoE performs worse than the best single model, our MoCaE boosts the segmentation AP by* 2.3. This is again significant improvement as it corresponds to $\sim 10\%$ relative gain compared to the best model. Also, the detection AP (AP_{box}) improves by 2.5 aligned with our findings in Sec. 4.1. Finally, MoCaE outperforms the single models in terms of all AP variants (e.g.,

Table 3. Comparison of our MoCAE with DEs and Vanilla MoE. MoEs obtained by our MoCAE outperforms DEs significantly even with less detectors. Our gains in green are obtained compared to the best single model for each performance measure, represented as underlined.

Model Type	Detector	AP	AP_{50}	AP_{75}	AP_S	AP_M	AP_L
Single Models	RS R-CNN	42.4	62.1	46.2	26.8	46.3	56.9
	ATSS	43.1	61.5	47.1	27.8	47.5	54.2
	PAA	43.2	60.8	47.1	27.0	47.0	57.6
Deep Ensembles	RS R-CNN × 5	44.5	63.0	49.1	28.8	48.6	58.4
	ATSS × 5	44.6	62.2	48.9	29.8	49.5	56.7
	PAA × 5	45.0	61.8	49.3	29.4	49.6	**59.9**
Mixtures of Experts	Vanilla MoE with Ref. NMS (RS R-CNN, ATSS, PAA)	44.4	62.6	48.2	27.8	48.4	**59.3**
	MoCAE (ATSS and PAA) - Ours	44.8	62.4	49.2	29.4	49.1	57.6
	MoCAE (RS R-CNN, ATSS, PAA) - Ours	**45.5**	**63.2**	**50.0**	**29.7**	**49.7**	**59.3**
		+2.3	+2.1	+2.9	+1.9	+2.2	+1.6

Table 4. Object detection performance on COCO *test-dev* and *mini-test* using strong object detectors. The gains are reported compared to the best single model as underlined. MoCAE maintains the significant AP boost also for this challenging setting as well.

Method	Pretraining Data	Backbone	COCO test-dev AP	AP_{50}	AP_{75}	AP_S	AP_M	AP_L	COCO minitest AP	AP_{50}	AP_{75}	AP_S	AP_M	AP_L
YOLOv7 [60]	None	L-size conv.	55.5	73.0	60.6	37.9	58.8	67.7	55.6	73.1	60.6	41.2	60.4	69.5
QueryInst [17]	None	Swin-L	55.7	75.7	61.4	36.2	58.4	70.9	55.9	75.4	61.3	38.5	60.8	73.2
DyHead [13]	ImageNet22K	Swin-L	56.6	75.5	61.8	39.4	59.8	68.7	56.8	75.6	62.2	42.8	60.6	71.0
Vanilla MoE	N/A	N/A	57.6	76.6	63.2	40.0	60.9	70.8	57.7	76.3	62.9	42.6	62.7	72.8
			+1.0	+0.9	+1.4	+0.6	+1.1	−0.1	+0.9	+0.7	+0.7	−0.2	+1.9	−0.4
MoCAE (Ours)	N/A	N/A	**59.0**	**77.2**	**64.7**	**41.1**	**62.6**	**72.4**	**58.9**	**76.8**	**64.3**	**44.7**	**63.6**	**74.1**
			+2.4	+1.5	+2.9	+1.7	+2.8	+1.5	+2.1	+1.1	+2.1	+1.9	+2.8	+1.1

Table 5. Instance segmentation performance on LVIS val set. While Vanilla MoE does not improve AP compared to the best single detector (underlined), MoCAE yields 2.3 AP gain over single detectors. AP_{box} represents detection AP.

Method	AP	AP_{50}	AP_{75}	AP_r	AP_c	AP_f	AP_{box}
Mask R-CNN [22]	25.4	39.2	27.3	15.7	24.7	30.4	26.6
RS Loss [52]	25.1	38.2	26.8	16.5	24.3	29.9	25.8
Seesaw Loss [62]	25.4	39.5	26.9	15.8	24.7	30.4	25.6
Vanilla MoE	25.2	38.3	26.8	16.5	24.3	29.9	25.9
	−0.2	−1.2	−0.5	0.0	−0.4	−0.5	−0.7
MoCAE (Ours)	**27.7**	**42.8**	**29.4**	**18.2**	**27.3**	**32.4**	**29.1**
	+2.3	+3.3	+2.1	+1.7	+2.4	+2.0	+2.5

Table 6. Rotated object detection performance on DOTA test set. AP_{50} is used following DOTA. MoCAE outperforms previous SOTA as it mainly improves the classes where the detectors have the lowest AP_{50}. See App. B for all classes.

Method	AP_{50}	5 Classes with Lowest Performance				
		Bridge	Soccer	Roundab.	Harbor	Helico.
RTMDet [46]	81.32	58.50	72.12	70.85	81.16	77.24
LSKN [40]	81.85	61.47	71.67	71.35	79.19	80.85
Vanilla MoE	80.60	**61.77**	70.98	65.92	84.28	77.57
	−1.25	+0.30	−1.14	−5.43	+3.12	−3.28
MoCAE (Ours)	**82.62**	61.38	**75.50**	**74.12**	**84.49**	**81.93**
	+0.77	−0.09	+3.38	+2.77	+3.33	+1.08

AP_r), thereby enabling a strong MoE in which the detectors complement each other.

Rotated Object Detection We now investigate MoCAE for rotated object detection on DOTA v1.0 dataset [63] with 15 classes. DOTA is also a challenging dataset comprising of aerial images with 67.1 objects on average. We use all 458 images in the val set to calibrate the detectors and report AP_{50} on the test set by submitting our results to the evaluation server. We combine LSKN [40] as the current SOTA and RTMDet [46] as two recent detectors. Following the literature, we use NMS with an IoU threshold of 0.35 as Soft NMS and Score Voting are not straightforward to use in this task.

Tab. 6 suggests that *we establish a new SOTA* with 82.62 AP_{50} on DOTA; improving the previous SOTA by 0.77. Having examined the classes, we note that our improvement originates mostly from the classes with relatively lower performance. For example, on 'soccer-field', 'roundabout', 'harbor' classes where the single detectors have between $70-80$ AP_{50}, the gain is around 3 AP_{50}. These gains enable us to demonstrate the ability of MoCAE to set a new SOTA in rotated object detection.

Table 7. AP and LAECE of uncalibrated, early and late calibrated models on COCO *mini-test*. Calibrator is N/A for baseline. Red: A notable AP drop, green: consistent AP, **bold**: best LAECE, underlined: second in LAECE.

Cal. Type	Calibrator	AP			LAECE		
		RS R-CNN	ATSS	PAA	RS R-CNN	ATSS	PAA
Early	N/A	42.4	43.1	43.2	13.79	0.20	3.39
	CW LR	26.4	42.0	37.1	0.44	0.12	0.22
	CW IR	41.9	42.8	42.5	**0.03**	**0.02**	1.39
	CA LR	42.4	42.8	43.2	0.65	0.17	0.37
	CA IR	42.4	43.1	43.2	0.14	0.10	**0.14**
Late	N/A	42.4	43.1	43.2	36.45	5.01	11.23
	CW LR	42.4	43.1	43.2	4.36	2.69	1.39
	CW IR	41.8	42.5	42.4	**1.56**	**2.35**	**1.21**
	CA LR	42.4	43.0	43.2	5.83	4.46	1.63
	CA IR	42.3	43.1	43.2	3.15	4.51	1.62

Table 8. Ablation analysis of MOCAE. We use the MoE combining RS R-CNN, ATSS and PAA on COCO *mini-test*. Calibration, either early or late, yields the major improvement, Soft NMS contributes slightly and Score Voting has a notable effect on the performance.

Cal. Type	Calibration	Refining NMS		AP
		Soft NMS	Score Voting	
Early	✗	✗	✗	43.3
Early	✓	✗	✗	44.5
Late	✓	✗	✗	44.7
Late	✓	✓	✗	44.8
Late	✗	✓	✗	43.4
Late	✓	✓	✓	44.4
Late	✓	✓	✓	**45.5**

4.3. Further Analyses and Discussions

Validating the Calibrator We first justify why we prefer Class-agnostic (CA) IR calibrator in MOCAE . We would ideally expect a calibrator to improve the calibration also by preserving the accuracy of the detector. To see that, we investigate LR and IR both CA and Class-wise (CW) on late as well as early calibration in Tab. 7. We observe in the red cells in Tab. 7 that all calibrators, except CA IR, decrease AP especially for early calibration. Furthermore, CA IR improves LAECE in all cases. We also discuss in App. B that CA IR improves average and maximum calibration errors; thereby providing a better gain for MoEs compared to other calibrators. These observations on accuracy and calibration led us to choose CA IR while calibrating the single models in MOCAE.

Ablation Analysis Now, we provide further ablation of MOCAE in Tab. 8. Note that regardless of early or late, calibration appears to be the major factor of the performance gain. Seeing that the late calibration performs slightly better than early (44.7 vs. 44.5) and it is simpler to implement, we use late calibration in MOCAE. Please see App.B for more results comparing early and late calibration. Tab. 8 shows that Soft NMS yields a small gain of 0.1 AP and Score Voting, combining boxes from different detectors to extract a new bounding box, improves AP notably from 44.8 to 45.5.

Early calibration reduces the sensitivity to background removal threshold Before we conclude, we investigate an additional use-case of early calibration in which it reduces the sensitivity of the detectors to background removal threshold in terms of both AP and efficiency. As AP provably benefits from more detections [54], detectors prefer a small background removal threshold as the first step of post-processing (Fig. 3(b)). *To illustrate,* 0.05 *is the common choice for COCO [27, 56, 69] and it is as low as* 10^{-4} *for LVIS [8, 20].* While this convention is preferred by AP, it can easily increase NMS processing time especially for over-confident detectors. This is because, for such detectors, the background removal step accepts redundant true-negatives (TNs), which should have been rejected. Hence, due to this large number of redundant TNs propagated to the NMS, NMS processing time significantly increases. To illustrate on PAA, which uses a threshold of 0.05 for COCO, NMS takes 29.2 ms/image on a Nvidia 1080Ti GPU, while it only takes $\sim$ 0.6 ms/image for ATSS and Faster R-CNN (F R-CNN). This difference among the detectors can easily be noticed by comparing the areas of the dots at 0.05 in Fig. 4(a). Specifically, we observed for PAA that $\sim$ 45K detections are propagated to the NMS per image on average. After early calibration, this number of detections from the same threshold reduces to $\sim$ 2K per image, which now enables NMS to take only 0.8 ms/image as ideally expected. Fig. 4(b) presents that NMS takes consistently between 0.6 to 0.8 ms/image for all detectors as the behaviour of the detectors are aligned.

Limitations One limitation of MOCAE stems from using multiple models during inference, which is also the case for DEs. Still, as each detector can process the input in parallel, the overhead introduced by MOCAE would be negligible when a separate GPU is allocated for each detector. Besides, comparing Fig. 2(b) with Fig. 2(a), we showed that calibration balances the contribution of the detectors to MoE. However, PAA, as the most accurate detector. has still the lowest contribution with %25.61 in Fig. 2(b). This is because LAECE after calibration in Tab. 1(Top) is still non-zero for the detectors. Therefore, better calibration methods could give rise to more accurate MoEs.

5. Conclusions

We showed that the incompatibility of the confidences across the detectors is the major challenge to obtain MoEs in object detection. To address this, we introduced MOCAE as a simple, principled and effective approach. MOCAE combines post-hoc calibration methods such as IR with an aggregation

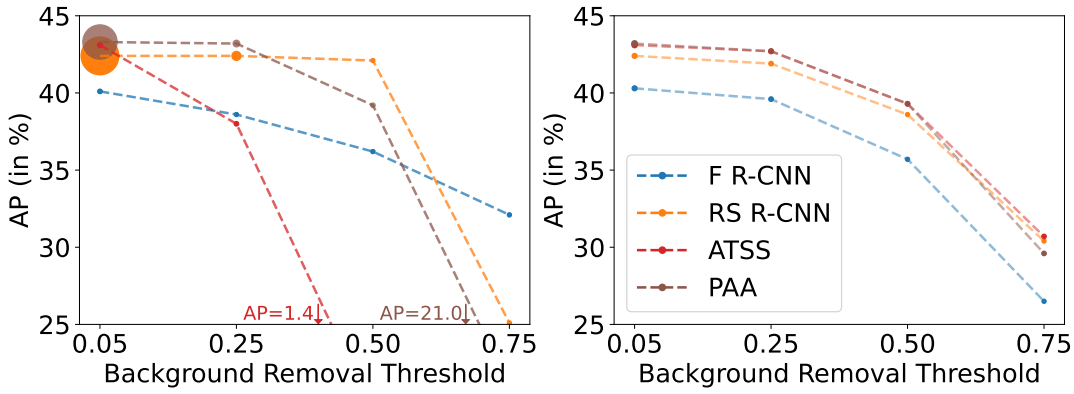

(a) Uncalibrated (b) Early Calibrated

Figure 4. The effect of background removal threshold on AP and NMS processing time for **(a)** uncalibrated and **(b)** early calibrated detectors on COCO. The area of the dots are proportional to the NMS processing time of the detectors. This threshold is typically set to 0.05, in which case PAA and RS R-CNN have large NMS processing time in **(a)**. Please see text for the discussion.

step which can be implemented by NMS. Specifically via calibration, we aligned the confidence with the IoU of the detection with the object that it overlaps the most. We showed that this is a useful calibration target, resulting in accurate MoEs with consistent gains across different detection tasks.

References

[1] Navaneeth Bodla, Bharat Singh, Rama Chellappa, and Larry S. Davis. Soft-nms – improving object detection with one line of code. In *IEEE/CVF International Conference on Computer Vision (ICCV)*, 2017. 1, 5, 13

[2] Daniel Bolya, Chong Zhou, Fanyi Xiao, and Yong Jae Lee. Yolact: Real-time instance segmentation. In *IEEE/CVF International Conference on Computer Vision (ICCV)*, 2019. 3

[3] Daniel Bolya, Sean Foley, James Hays, and Judy Hoffman. Tide: A general toolbox for identifying object detection errors. In *The IEEE European Conference on Computer Vision (ECCV)*, 2020. 19

[4] Holger Caesar, Varun Bankiti, Alex H. Lang, Sourabh Vora, Venice Erin Liong, Qiang Xu, Anush Krishnan, Yu Pan, Giancarlo Baldan, and Oscar Beijbom. nuscenes: A multimodal dataset for autonomous driving. In *IEEE/CVF Conference on Computer Vision and Pattern Recognition (CVPR)*, 2020. 1

[5] Zhaowei Cai and Nuno Vasconcelos. Cascade R-CNN: Delving into high quality object detection. In *IEEE/CVF Conference on Computer Vision and Pattern Recognition (CVPR)*, 2018. 3

[6] Nicolas Carion, Francisco Massa, Gabriel Synnaeve, Nicolas Usunier, Alexander Kirillov, and Sergey Zagoruyko. End-to-end object detection with transformers. In *European Conference on Computer Vision (ECCV)*, 2020. 3

[7] Ángela Casado-García and Jónathan Heras. Ensemble methods for object detection. In *European Conference on Artificial Intelligence*, 2020. 1, 3

[8] Kai Chen, Jiaqi Wang, Jiangmiao Pang, Yuhang Cao, Yu Xiong, Xiaoxiao Li, Shuyang Sun, Wansen Feng, Ziwei Liu, Jiarui Xu, Zheng Zhang, Dazhi Cheng, Chenchen Zhu, Tianheng Cheng, Qijie Zhao, Buyu Li, Xin Lu, Rui Zhu, Yue Wu, Jifeng Dai, Jingdong Wang, Jianping Shi, Wanli Ouyang, Chen Change Loy, and Dahua Lin. MMDetection: Open mmlab detection toolbox and benchmark. *arXiv*, 1906.07155, 2019. 8, 14

[9] Kean Chen, Weiyao Lin, Jianguo li, John See, Ji Wang, and Junni Zou. Ap-loss for accurate one-stage object detection. *IEEE Transactions on Pattern Analysis and Machine Intelligence (TPAMI)*, pages 1–1, 2020. 1

[10] Yukang Chen, Yanwei Li, Tao Kong, Lu Qi, Ruihang Chu, Lei Li, and Jiaya Jia. Scale-aware automatic augmentation for object detection. In *IEEE Conference on Computer Vision and Pattern Recognition (CVPR)*, 2021. 1

[11] Jiacheng Cheng and Nuno Vasconcelos. Calibrating deep neural networks by pairwise constraints. In *Proceedings of the IEEE/CVF Conference on Computer Vision and Pattern Recognition (CVPR)*, 2022. 3

[12] Jifeng Dai, Yi Li, Kaiming He, and Jian Sun. R-FCN: Object detection via region-based fully convolutional networks. In *Advances in Neural Information Processing Systems (NeurIPS)*, 2016. 3, 14

[13] Xiyang Dai, Yinpeng Chen, Bin Xiao, Dongdong Chen, Mengchen Liu, Lu Yuan, and Lei Zhang. Dynamic head: Unifying object detection heads with attentions. In *Proceedings of the IEEE/CVF Conference on Computer Vision and Pattern Recognition (CVPR)*, pages 7373–7382, 2021. 5, 7, 14

[14] Kaiwen Duan, Song Bai, Lingxi Xie, Honggang Qi, Qingming Huang, and Qi Tian. Centernet: Keypoint triplets for object detection. In *IEEE/CVF International Conference on Computer Vision (ICCV)*, 2019. 3

[15] Debidatta Dwibedi, Ishan Misra, and Martial Hebert. Cut, paste and learn: Surprisingly easy synthesis for instance detection. In *IEEE/CVF International Conference on Computer Vision (ICCV)*, 2017. 1

[16] Haoshu Fang, Jianhua Sun, Runzhong Wang, Minghao Gou, Yong-Lu Li, and Cewu Lu. Instaboost: Boosting instance segmentation via probability map guided copy-pasting. *2019 IEEE/CVF International Conference on Computer Vision (ICCV)*, pages 682–691, 2019. 1

[17] Yuxin Fang, Shusheng Yang, Xinggang Wang, Yu Li, Chen Fang, Ying Shan, Bin Feng, and Wenyu Liu. Instances as queries. In *Proceedings of the IEEE/CVF International Conference on Computer Vision (ICCV)*, pages 6910–6919, 2021. 5, 7, 14

[18] Andreas Geiger, Philip Lenz, and Raquel Urtasun. Are we ready for autonomous driving? the kitti vision benchmark suite. In *Conference on Computer Vision and Pattern Recognition (CVPR)*, 2012. 1

[19] Chuan Guo, Geoff Pleiss, Yu Sun, and Kilian Q. Weinberger. On calibration of modern neural networks. In *Proceedings of the 34th International Conference on Machine Learning*, pages 1321–1330. PMLR, 2017. 3, 4, 15

[20] Agrim Gupta, Piotr Dollar, and Ross Girshick. Lvis: A dataset for large vocabulary instance segmentation. In *The IEEE Conference on Computer Vision and Pattern Recognition (CVPR)*, 2019. 3, 6, 8

[21] Kaiming He, Xiangyu Zhang, Shaoqing Ren, and Jian Sun. Deep residual learning for image recognition. In *IEEE/CVF Conference on Computer Vision and Pattern Recognition (CVPR)*, 2016. 5, 14

[22] Kaiming He, Georgia Gkioxari, Piotr Dollar, and Ross Girshick. Mask R-CNN. In *IEEE/CVF International Conference on Computer Vision (ICCV)*, 2017. 1, 6, 7, 14, 20

[23] Yihui He, Chenchen Zhu, Jianren Wang, Marios Savvides, and Xiangyu Zhang. Bounding box regression with uncertainty for accurate object detection. In *IEEE/CVF Conference on Computer Vision and Pattern Recognition (CVPR)*, 2019. 13

[24] Zhaojin Huang, Lichao Huang, Yongchao Gong, Chang Huang, and Xinggang Wang. Mask scoring r-cnn. In *IEEE/CVF Conference on Computer Vision and Pattern Recognition (CVPR)*, 2019. 3

[25] Borui Jiang, Ruixuan Luo, Jiayuan Mao, Tete Xiao, and Yuning Jiang. Acquisition of localization confidence for accurate object detection. In *The European Conference on Computer Vision (ECCV)*, 2018. 1, 3, 4

[26] Fehmi Kahraman, Kemal Oksuz, Sinan Kalkan, and Emre Akbas. Correlation loss: Enforcing correlation between classification and localization. In *Association for the Advancement of Artificial Intelligence (AAAI)*, 2023. 4

[27] Kang Kim and Hee Seok Lee. Probabilistic anchor assignment with iou prediction for object detection. In *The European Conference on Computer Vision (ECCV)*, 2020. 1, 3, 5, 8, 13, 14

[28] Alexander Kirillov, Eric Mintun, Nikhila Ravi, Hanzi Mao, Chloe Rolland, Laura Gustafson, Tete Xiao, Spencer Whitehead, Alexander C. Berg, Wan-Yen Lo, Piotr Dollár, and Ross Girshick. Segment anything. *arXiv:2304.02643*, 2023. 1

[29] Volodymyr Kuleshov, Nathan Fenner, and Stefano Ermon. Accurate uncertainties for deep learning using calibrated regression. In *International Conference on Machine Learning (ICML)*, 2018. 4

[30] Ananya Kumar, Percy S Liang, and Tengyu Ma. Verified uncertainty calibration. In *Advances in Neural Information Processing Systems (NeurIPS)*, 2019. 3

[31] Fabian Kuppers, Jan Kronenberger, Amirhossein Shantia, and Anselm Haselhoff. Multivariate confidence calibration for object detection. In *The IEEE/CVF Conference on Computer Vision and Pattern Recognition (CVPR) Workshops*, 2020. 3, 5

[32] Fabian Kuppers, Jonas Schneider, and Anselm Haselhoff. Parametric and multivariate uncertainty calibration for regression and object detection. In *Safe Artificial Intelligence for Automated Driving Workshop in The European Conference on Computer Vision*, 2022. 5

[33] Alina Kuznetsova, Hassan Rom, Neil Alldrin, Jasper R. R. Uijlings, Ivan Krasin, Jordi Pont-Tuset, Shahab Kamali, Stefan Popov, Matteo Malloci, Tom Duerig, and Vittorio Ferrari. The open images dataset V4: unified image classification, object detection, and visual relationship detection at scale. *arXiv*, 1811.00982, 2018. 1

[34] Balaji Lakshminarayanan, Alexander Pritzel, and Charles Blundell. Simple and scalable predictive uncertainty estimation using deep ensembles. In *Advances in Neural Information Processing Systems*, 2017. 1

[35] Hei Law and Jia Deng. Cornernet: Detecting objects as paired keypoints. In *The European Conference on Computer Vision (ECCV)*, 2018. 3

[36] Hyungtae Lee, Sungmin Eum, and Heesung Kwon. Me r-cnn: Multi-expert r-cnn for object detection. *IEEE Transactions on Image Processing*, 29:1030–1044, 2020. 1

[37] Xiang Li, Wenhai Wang, Xiaolin Hu, Jun Li, Jinhui Tang, and Jian Yang. Generalized focal loss v2: Learning reliable localization quality estimation for dense object detection. In *IEEE/CVF Conference on Computer Vision and Pattern Recognition (CVPR)*, 2019. 1, 4

[38] Xiang Li, Wenhai Wang, Lijun Wu, Shuo Chen, Xiaolin Hu, Jun Li, Jinhui Tang, and Jian Yang. Generalized focal loss: Learning qualified and distributed bounding boxes for dense object detection. In *Advances in Neural Information Processing Systems (NeurIPS)*, 2020. 1, 4

[39] Yanghao Li, Hanzi Mao, Ross Girshick, and Kaiming He. Exploring plain vision transformer backbones for object detection. In *European Conference on Computer Vision (ECCV)*, 2022. 1

[40] Yuxuan Li, Qibin Hou, Zhaohui Zheng, Mingming Cheng, Jian Yang, and Xiang Li. Large selective kernel network for remote sensing object detection. *ArXiv*, 2023. 7, 14

[41] Tsung-Yi Lin, Piotr Dollár, Ross B. Girshick, Kaiming He, Bharath Hariharan, and Serge J. Belongie. Feature pyramid networks for object detection. In *IEEE/CVF Conference on Computer Vision and Pattern Recognition (CVPR)*, 2017. 5, 14

[42] Tsung-Yi Lin, Priya Goyal, Ross B. Girshick, Kaiming He, and Piotr Dollár. Focal loss for dense object detection. In *IEEE/CVF International Conference on Computer Vision (ICCV)*, 2017. 1

[43] Tsung-Yi Lin, Michael Maire, Serge Belongie, James Hays, Pietro Perona, Deva Ramanan, Piotr Dollár, and C Lawrence Zitnick. Microsoft COCO: Common Objects in Context. In *The European Conference on Computer Vision (ECCV)*, 2014. 2, 3, 5

[44] Tsung-Yi Lin, Priya Goyal, Ross Girshick, Kaiming He, and Piotr Dollár. Focal loss for dense object detection. *IEEE*

Transactions on Pattern Analysis and Machine Intelligence (TPAMI), 42(2):318–327, 2020. 1, 3

[45] Ze Liu, Yutong Lin, Yue Cao, Han Hu, Yixuan Wei, Zheng Zhang, Stephen Lin, and Baining Guo. Swin transformer: Hierarchical vision transformer using shifted windows. In *Proceedings of the IEEE/CVF International Conference on Computer Vision (ICCV)*, 2021. 1, 5, 14

[46] Chengqi Lyu, Wenwei Zhang, Haian Huang, Yue Zhou, Yudong Wang, Yanyi Liu, Shilong Zhang, and Kai Chen. Rtmdet: An empirical study of designing real-time object detectors. *ArXiv*, 2022. 7

[47] Jishnu Mukhoti, Viveka Kulharia, Amartya Sanyal, Stuart Golodetz, Philip Torr, and Puneet Dokania. Calibrating deep neural networks using focal loss. In *Advances in Neural Information Processing Systems*, pages 15288–15299. Curran Associates, Inc., 2020. 3

[48] Lukás Neumann, Andrew Zisserman, and Andrea Vedaldi. Relaxed softmax: Efficient confidence auto-calibration for safe pedestrian detection. In *NIPS MLITS Workshop on Machine Learning for Intelligent Transportation System*, 2018. 3

[49] Jeremy Nixon, Michael W. Dusenberry, Linchuan Zhang, Ghassen Jerfel, and Dustin Tran. Measuring calibration in deep learning. In *IEEE/CVF Conference on Computer Vision and Pattern Recognition (CVPR) Workshops*, 2019. 3

[50] Kemal Oksuz, Baris Can Cam, Emre Akbas, and Sinan Kalkan. Localization recall precision (LRP): A new performance metric for object detection. In *The European Conference on Computer Vision (ECCV)*, 2018. 19

[51] Kemal Oksuz, Baris Can Cam, Emre Akbas, and Sinan Kalkan. A ranking-based, balanced loss function unifying classification and localisation in object detection. In *Advances in Neural Information Processing Systems (NeurIPS)*, 2020. 1

[52] Kemal Oksuz, Baris Can Cam, Emre Akbas, and Sinan Kalkan. Rank & sort loss for object detection and instance segmentation. In *The International Conference on Computer Vision (ICCV)*, 2021. 1, 3, 6, 7, 14, 20

[53] Kemal Oksuz, Baris Can Cam, Sinan Kalkan, and Emre Akbas. One metric to measure them all: Localisation recall precision (lrp) for evaluating visual detection tasks. *IEEE Transactions on Pattern Analysis and Machine Intelligence*, pages 1–1, 2021. 19

[54] Kemal Oksuz, Tom Joy, and Puneet Dokania. Towards building self-aware object detectors via reliable uncertainty quantification and calibration. In *IEEE/CVF Conference on Computer Vision and Pattern Recognition (CVPR)*, 2023. 3, 5, 8, 14, 15

[55] Francesco Pinto, Philip H. S. Torr, and Puneet K. Dokania. An impartial take to the cnn vs transformer robustness contest. In *The European Conference on Computer Vision (ECCV)*, 2022. 3

[56] Shaoqing Ren, Kaiming He, Ross Girshick, and Jian Sun. Faster R-CNN: Towards real-time object detection with region proposal networks. *IEEE Transactions on Pattern Analysis and Machine Intelligence (TPAMI)*, 39(6):1137–1149, 2017. 3, 8, 14

[57] Peize Sun, Rufeng Zhang, Yi Jiang, Tao Kong, Chenfeng Xu, Wei Zhan, Masayoshi Tomizuka, Lei Li, Zehuan Yuan, Changhu Wang, and Ping Luo. SparseR-CNN: End-to-end object detection with learnable proposals. In *IEEE/CVF Conference on Computer Vision and Pattern Recognition (CVPR)*, 2018. 3

[58] Pei Sun, Henrik Kretzschmar, Xerxes Dotiwalla, Aurelien Chouard, Vijaysai Patnaik, Paul Tsui, James Guo, Yin Zhou, Yuning Chai, Benjamin Caine, Vijay Vasudevan, Wei Han, Jiquan Ngiam, Hang Zhao, Aleksei Timofeev, Scott Ettinger, Maxim Krivokon, Amy Gao, Aditya Joshi, Yu Zhang, Jonathon Shlens, Zhifeng Chen, and Dragomir Anguelov. Scalability in perception for autonomous driving: Waymo open dataset. In *IEEE/CVF Conference on Computer Vision and Pattern Recognition (CVPR)*, 2020. 1

[59] Zhi Tian, Chunhua Shen, Hao Chen, and Tong He. Fcos: Fully convolutional one-stage object detection. In *IEEE/CVF International Conference on Computer Vision (ICCV)*, 2019. 1, 3

[60] Chien-Yao Wang, Alexey Bochkovskiy, and Hong-Yuan Mark Liao. YOLOv7: Trainable bag-of-freebies sets new state-of-the-art for real-time object detectors. *arXiv preprint arXiv:2207.02696*, 2022. 5, 7, 14

[61] Deng-Bao Wang, Lei Feng, and Min-Ling Zhang. Rethinking calibration of deep neural networks: Do not be afraid of overconfidence. In *Advances in Neural Information Processing Systems (NeurIPS)*, 2021. 3

[62] Jiaqi Wang, Wenwei Zhang, Yuhang Zang, Yuhang Cao, Jiangmiao Pang, Tao Gong, Kai Chen, Ziwei Liu, Chen Change Loy, and Dahua Lin. Seesaw loss for long-tailed instance segmentation. *2021 IEEE/CVF Conference on Computer Vision and Pattern Recognition (CVPR)*, pages 9690–9699, 2020. 1, 6, 7, 14, 20

[63] Gui-Song Xia, Xiang Bai, Jian Ding, Zhen Zhu, Serge Belongie, Jiebo Luo, Mihai Datcu, Marcello Pelillo, and Liangpei Zhang. Dota: A large-scale dataset for object detection in aerial images. In *The IEEE Conference on Computer Vision and Pattern Recognition (CVPR)*, 2018. 1, 3, 7

[64] Saining Xie, Ross B. Girshick, Piotr Dollár, Zhuowen Tu, and Kaiming He. Aggregated residual transformations for deep neural networks. *arXiv*, 1611.05431, 2016. 6, 14

[65] Ke Yan, Xiaosong Wang, Le Lu, and Ronald M. Summers. "deeplesion: Automated mining of large-scale lesion annotations and universal lesion detection with deep learning". *Journal of Medical Imaging*, 5(3), 2018. 1

[66] Bianca Zadrozny and Charles Elkan. Transforming classifier scores into accurate multiclass probability estimates. In *Proceedings of the eighth ACM SIGKDD international conference on Knowledge discovery and data mining*, pages 694–699, 2002. 1, 4

[67] Hongkai Zhang, Hong Chang, Bingpeng Ma, Naiyan Wang, and Xilin Chen. Dynamic r-cnn: Towards high quality object detection via dynamic training. In *The European Conference on Computer Vision (ECCV)*, 2020. 14

[68] Haoyang Zhang, Ying Wang, Feras Dayoub, and Niko Sünderhauf. Varifocalnet: An iou-aware dense object detector. In *IEEE/CVF Conference on Computer Vision and Pattern Recognition (CVPR)*, 2021. 1

[69] Shifeng Zhang, Cheng Chi, Yongqiang Yao, Zhen Lei, and Stan Z. Li. Bridging the gap between anchor-based and anchor-free detection via adaptive training sample selection. In *IEEE/CVF Conference on Computer Vision and Pattern Recognition (CVPR)*, 2020. 1, 3, 4, 8, 14

[70] Shiyu Zhao, Zhixing Zhang, Samuel Schulter, Long Zhao, BG Vijay Kumar, Anastasis Stathopoulos, Manmohan Chandraker, and Dimitris N Metaxas. Exploiting unlabeled data with vision and language models for object detection. In *European Conference on Computer Vision (ECCV)*, 2022. 1

[71] Xizhou Zhu, Weijie Su, Lewei Lu, Bin Li, Xiaogang Wang, and Jifeng Dai. Deformable {detr}: Deformable transformers for end-to-end object detection. In *International Conference on Learning Representations (ICLR)*, 2021. 3

[72] Barret Zoph, Ekin Dogus Cubuk, Golnaz Ghiasi, Tsung-Yi Lin, Jonathon Shlens, and Quoc V. Le. Learning data augmentation strategies for object detection. In *European Conference on Computer Vision (ECCV)*, 2020. 1

[73] Barret Zoph, Golnaz Ghiasi, Tsung-Yi Lin, Yin Cui, Hanxiao Liu, Ekin Dogus Cubuk, and Quoc Le. Rethinking pre-training and self-training. In *Advances in Neural Information Processing Systems*, pages 3833–3845. Curran Associates, Inc., 2020. 1

APPENDICES

Contents

A. Further Details on Refining NMS

As described in Sec. 3.1.2, we combine *Soft NMS* with *Score Voting* while aggregating the detections of different detectors in our MoCaE approach. Here, for the sake of completeness, we present these approaches.

Let's start with the standard NMS and provide some background information. Basically, given a set of raw detections after background removal (Sec. 2), the standard NMS first selects the maximum-scoring detection $\{\hat{b}_\alpha, \hat{p}_\alpha\}$ and then groups the detections that have an IoU with $\{\hat{b}_\alpha, \hat{p}_\alpha\}$ larger than a predefined IoU threshold[1]. Then, NMS survives $\{\hat{b}_\alpha, \hat{p}_\alpha\}$ by placing it to the final detection set and discards all other raw detections from that group assuming that they are duplicates. This process takes place until all raw detections are either moved to the final detection set or discarded. Instead of removing the detections (i.e., the detections other than $\{\hat{b}_\alpha, \hat{p}_\alpha\}$) completely, Soft NMS decreases their confidence scores as a function of their overlap with $\{\hat{b}_\alpha, \hat{p}_\alpha\}$. More specifically, Soft NMS has two variants determined by the type of this rescoring function. The first one is called *Linear Soft NMS*, in which the confidence scores are rescored such that

$$\hat{p}_i = \begin{cases} \hat{p}_i & \text{if } \mathrm{IoU}(\hat{b}_i, \hat{b}_\alpha) < \mathrm{IoU}_{NMS} \\ \hat{p}_i \times (1 - \mathrm{IoU}(\hat{b}_i, \hat{b}_\alpha)) & \text{else,} \end{cases} \tag{A.5}$$

where IoU_{NMS} is the predefined IoU threshold for NMS, set to 0.30 in [1]. Note that Eq. (A.5) corresponds to the standard NMS if $\hat{p}_i$ is set to 0 for the case that $\mathrm{IoU}(\hat{b}_i, \hat{b}_\alpha) \geq \mathrm{IoU}_{NMS}$ in which $\hat{b}_i$ overlaps with $\hat{b}_\alpha$ more than a threshold. Differently, Soft NMS decreases the score $\hat{p}_i$ by considering the overlap of $\hat{b}_i$ with $\hat{b}_\alpha$. In the case of a higher overlap, the score $\hat{p}_i$ is reduced more with the intuition that $\hat{b}_i$ is more likely to detect the same object with $\hat{b}_\alpha$. With the same intuition, the second Soft NMS variant, for *Gaussian Soft NMS* modifies the scores as follows,

$$\hat{p}_i = \hat{p}_i e^{-\frac{\mathrm{IoU}(\hat{b}_i, \hat{b}_\alpha)^2}{\sigma_{\mathrm{NMS}}}}, \tag{A.6}$$

where σ_{NMS} is a hyper-parameter to control how much to suppress the scores such that a smaller σ_{NMS} implies that $\hat{p}_i$ is suppressed more. We provide experiments on how σ_{NMS} affects the performance and find that $\sigma_{\mathrm{NMS}} \in [0.40, 0.60]$ typically performs well for MoCaE. Therefore, as Soft NMS is less rigid in removing overlapping detections, it naturally leads to improved recall.

Next we discuss Score Voting[27], which aims to refine the final detections after NMS (or Soft NMS). Inspired by [23], the bounding box of a final detection is refined by utilizing the raw detections and their confidence. Specifically, the refined box $\hat{b}_i$ is obtained as the weighted average of raw bounding boxes $\hat{b}_j$ (i.e., before NMS) as follows,

$$\hat{b}_i = \frac{\sum_j \hat{p}_j \hat{IoU}_j \hat{b}_j}{\sum \hat{p}_j \hat{IoU}_j}, \tag{A.7}$$

where $\hat{IoU}_j$ is

$$\hat{IoU}_j = e^{-\frac{1-\mathrm{IoU}(\hat{b}_i, \hat{b}_j)^2}{\sigma_{\mathrm{SV}}}}, \tag{A.8}$$

such that σ_{SV} is the hyper-parameter of Score Voting, which we set to 0.04 in all of our experiments.

Note that while Soft NMS keeps the box as it is and updates the confidence score, Score Voting does the opposite by keeping the score as it is and refines the box. As a result, these two approaches adopted in Refining NMS complement each other well, enabling us to obtain a strong aggregator for MoCaE.

[1] Considering the common usage of NMS, we assume that NMS operates class-wise. Hence, the predicted class label is not explicitly included in the detection representation.

B. Further Experiments and Analyses

Here, we present further experiments and analyses that are not included in the main text due to space limitation.

B.1. Further Details on Used Models

We provide the details of the used models as follows. We again note that we haven't trained any model but used off-the-shelf detectors with the exception of DEs. Here we provide further details on the used detectors. Still, as it is not feasible to provide all of the details, we also present the papers and repositories that we borrow these off-the-shelf models in order to ensure the reproducibility of our results.

Object Detection We use two different configurations. In the first one, we employ three detectors with ResNet-50 [21] with FPN [41] backbone. These detectors are:

- Rank & Sort R-CNN (RS R-CNN) [52] is a recent representative of the two-stage R-CNN family [12, 56, 67] optimizing a ranking-based loss function,
- Adaptive Training Sample Selection (ATSS) [69] is a common one stage baseline,
- Probabilistic Anchor Assignment (PAA) [27] relies on the one-stage ATSS architecture but with a different anchor assignment mechanism and postprocessing of the confidence scores.

We obtain RS R-CNN and ATSS from [54] and PAA from [8]. All these detectors are trained for 36 epochs using multi-scale training data augmentation in which the shorter side of the image is resized within the range of [480, 800] for RS R-CNN and ATSS and [640, 800] for PAA. We do not use Soft NMS and Score Voting for the single detectors.

In our second setting, we use the following detectors:

- YOLOv7 [60] with a large convolutional backbone following its original setting,
- QueryInst [17] as a transformer-based detector with a Swin-L [45] backbone,
- ATSS with transformer-based dynamic head [13] and again Swin-L backbone.

Again, we obtain YOLOv7 and dynamic head from mmdetection [8] and use the official repository of QueryInst [17].

Instance Segmentation We use three different Mask R-CNN variants for instance segmentation:

- The vanilla Mask R-CNN [22] with ResNeXt-101 [64] backbone, softmax classifier and using Repeat Factor Sampling (RFS) to address the long-tailed nature of LVIS,
- Mask R-CNN with ResNet-50, sigmoid classifier, trained with RS Loss [52] and RFS,
- Mask R-CNN with ResNet-50, softmax classifier, trained with Seesaw Loss[62] but no RFS.

We obtain Vanilla Mask R-CNN and Seesaw Loss from mmdetection. As for Mask R-CNN trained with RS Loss, we use the official repository of RS Loss [52] in which it is trained for 12 epochs using multi-scale training augmentation. The other Mask R-CNN variants also employ multi-scale training augmentation and the Vanilla Mask R-CNN is trained for 12 epochs as well. Differently, Mask R-CNN with Seesaw Loss is trained for 24 epochs and uses the mask normalization technique proposed in the same paper[62].

Rotated Object Detection Finally for rotated object detection, we use RTMDet and LSKN as two different detectors. We obtain RTMDet again from mmdetection (which is also the official repository for RTMDet) and LSKN from its official repository [40].

B.2. Further Analyses on Calibration

Definitions of the Calibration Errors We introduce our calibration criterion in Eq. (4). This criterion requires the confidence of a detection to align with its IoU with the ground truth box that the detection overlaps the most. As aforementioned, computing the calibration error based on this criterion corresponds to using an IoU threshold of 0 to validate TPs. This is equivalent to using $\text{precision}^c(j) = 1$ for class c in Eq. (3), which then reduces to

$$\text{LaECE}^c = \sum_{j=1}^{J} \frac{|\hat{\mathcal{D}}_j^c|}{|\hat{\mathcal{D}}^c|} \left| \bar{p}_j^c - \bar{\text{IoU}}^c(j) \right|. \tag{A.9}$$

where $\hat{\mathcal{D}}^c$ denotes the set of detections for class c; $\hat{\mathcal{D}}_j^c$ is the set of detections in the jth bin for class c; $\bar{p}_j^c$ is the average confidence of the detections in $\hat{\mathcal{D}}_j^c$; and $\bar{\text{IoU}}^c(j)$ is the average IoU of the detections in $\hat{\mathcal{D}}_j^c$. Following [54], we use $J = 25$ and average over LaECE^c of classes for the detector LaECE.

In addition to LaECE, here we define Localisation-aware Average Calibration Error (LaACE) and Localisation-aware Maximum Calibration Error (LaMCE) similar to the way how Expected Calibration Error (ECE) is extended to Average Calibration and Maximum Calibration Errors. We find LaACE and LaMCE useful as they reduce the dominance of certain bins on the calibration error as in the case of LaECE. This is especially important for early calibration from which thousands of confidence scores are obtained from a single image, most of which have a confidence close to 0. Specifically, in our case, we define LaACE^c for class c as

$$\text{LaACE}^c = \sum_{j=1}^{J} \frac{1}{J} \left| \bar{p}_j^c - \bar{\text{IoU}}^c(j) \right|, \tag{A.10}$$

and LaMCE^c for class c as

$$\text{LaMCE}^c = \max_{j \in \{1,2,..,J\}} \left| \bar{p}_j^c - \bar{\text{IoU}}^c(j) \right|. \tag{A.11}$$

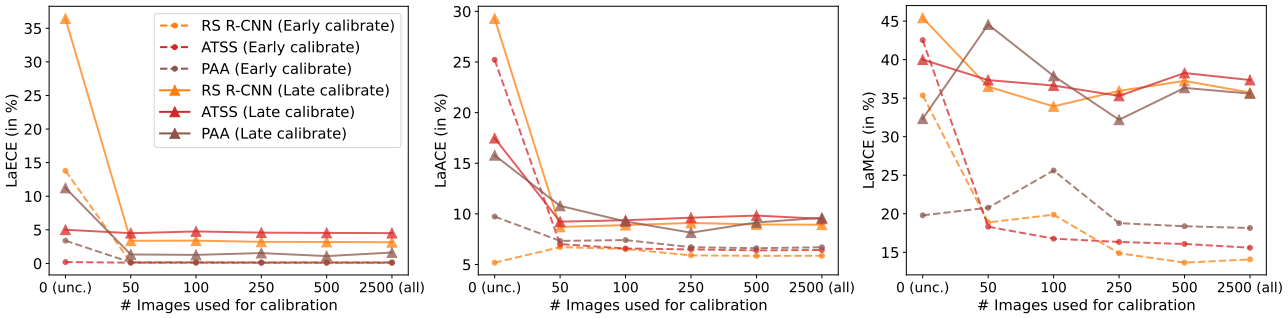

(a) LaECE (b) LaACE (c) LaMCE

Figure A.5. The effect of number of images on calibration using CA IR. We find it sufficient to use only 500 images for calibration.

Table A.9. Accuracy and calibration performance of uncalibrated, early calibrated and late calibrated models on COCO *mini-test*. A red cell indicates a notable AP drop compared to the uncalibrated detector while a green cell implies consistency. CW: Class-wise, CA: class-agnostic, bold: best calibration performance, underlined: second best. Calibrator is not available (N/A) for uncalibrated models. CA IR provides a good balance of AP and calibration performance.

Cal. Type	Class Type	Calibrator	AP			LaECE			LaACE			LaMCE		
			RS R-CNN	ATSS	PAA	RS R-CNN	ATSS	PAA	RS R-CNN	ATSS	PAA	RS R-CNN	ATSS	PAA
	N/A	N/A	42.4	43.1	43.2	13.79	0.20	3.39	**5.18**	25.22	9.73	35.37	42.53	19.80
Early Cal.	CW	LR	26.4	42.0	37.1	0.44	0.12	0.22	25.12	10.13	28.95	61.11	24.79	60.05
		IR	41.9	42.8	42.5	**0.03**	**0.02**	1.39	5.23	**5.40**	**5.26**	25.10	25.38	26.60
	CA	LR	42.4	42.8	43.2	0.65	0.17	0.37	27.48	7.86	25.49	68.81	23.07	54.03
		IR	42.4	43.1	43.2	0.14	0.10	**0.14**	5.86	6.43	6.70	**14.08**	**15.59**	**18.15**
	N/A	N/A	42.4	43.1	43.2	36.45	5.01	11.23	29.30	17.48	15.79	45.42	40.00	32.33
Late Cal.	CW	LR	42.4	43.1	43.2	4.36	2.69	1.39	14.19	**9.03**	12.01	40.20	**29.51**	33.76
		IR	41.8	42.5	42.4	**1.56**	**2.35**	**1.21**	9.21	9.81	**9.24**	38.43	40.34	37.84
	CA	LR	42.4	43.0	43.2	5.83	4.46	1.63	13.86	9.46	11.88	37.79	29.59	**29.91**
		IR	42.3	43.1	43.2	3.15	4.51	1.62	**8.93**	9.51	9.61	**35.72**	37.35	35.59

Following LaECE, we obtain LaACE and LaMCE for the detector by averaging over the classes.

We include the full version of accuracy and calibration performance comparison of different methods in Tab. A.9. This table further confirms our choice of CA IR as it improves LaACE and LaMCE in most of the cases.

500 Images are Sufficient for MoCaE Now we investigate how many images are sufficient for calibration to enable MoEs using MoCaE. Following the literature [19, 54], we learn a calibrator on a held-out validation set and then report the results on the test set. Our aim here is to determine the cardinality of the held-out validation set to properly calibrate the models. This can help the practitioners to avoid reserving redundant data for this held-out validation set. For this analysis, we learn calibrators on both early and late calibration setting by using different number of images. Fig. A.5 presents how LaECE, LaACE and LaMCE change when the cardinality of the hold-out validation set changes on three different detectors. We observe in general that calibration errors drop significantly even when only 50 images are used to learn the calibrators. With more images, while we do not observe a notable gain in LaECE (Fig. A.5(a)), LaACE (Fig. A.5(b)) and LaMCE (Fig. A.5(c)) continue to improve especially for early calibration, implying the necessity for these calibration errors. Overall, we haven't observed a notable gain after 500 images, hence we keep 500 images on the held-out validation set while training the calibrators.

Further Comparison of Early and Late Calibration Here, we provide further comparison on early and late calibration. In Tab. A.10, we can see that while both approaches improve single models, late calibration performs slightly better than early calibration consistently. Furthermore, practically speaking, late calibration is significantly simpler. This is because the number of confidence scores obtained before post-processing is significantly larger than that obtained after post-processing (i.e., final detections). To illustrate on RS R-CNN, which outputs 1K proposals for each image as raw detections, a single image results in 80K raw confidence scores for COCO dataset and more than 1M scores for LVIS as each proposal has a score for each class. Also considering that, a very large amount of these raw detections do not overlap with any object, the problem gets more challenging as well due to the imbalanced nature of the data. While we use RS R-CNN, a two-stage detector, as an example, the

Table A.10. Further experiments comparing early and late calibration. Standard NMS is used for both of the methods. While both approaches improve single models, late calibration performs slightly better.

Calibration Type	RS R-CNN	ATSS	PAA	AP	AP_{50}	AP_{75}	AP_S	AP_M	AP_L
N/A	✓			42.4	62.1	46.2	26.8	46.3	56.9
(Single		✓		43.1	61.5	47.1	27.8	47.5	54.2
Models)			✓	43.2	60.8	47.1	27.0	47.0	57.6
Early	✓	✓		43.9	63.5	47.9	28.6	47.9	56.9
Late	✓	✓		44.1	63.0	48.4	28.5	48.4	56.8
Early	✓		✓	43.8	63.3	47.7	28.1	47.8	57.6
Late	✓		✓	44.0	62.7	47.9	28.2	48.2	58.1
Early		✓	✓	44.3	63.1	47.8	28.8	48.1	56.7
Late		✓	✓	44.4	62.5	48.5	29.2	48.5	57.3
Early	✓	✓	✓	44.5	**63.7**	48.4	29.0	48.5	57.5
Late	✓	✓	✓	**44.7**	63.1	**48.9**	**29.2**	**49.0**	**58.2**

number of raw confidence scores is significantly larger for one-stage detectors which makes predictions directly from a very large number of anchors; making early calibration even more impractical for such detectors[2]. On the other hand, we use only top-100 detections in COCO and top-300 detections in LVIS for each image following the evaluation specification of these datasets. Thereby resulting in more practical scenarios with significantly smaller number of detections for late calibration compared to early. Consequently, considering its slight accuracy gain as well as simplicity, we prefer late calibration over early to obtain MoEs in MoCaE.

Effect of Different Calibration Methods on MoEs While we choose CA IR as our calibration method in MoCaE, here we present how different calibration methods perform in obtaining MoEs. Specifically, we use late calibration with CA LR and CW LR as these two methods also preserve the accuracy of single models as shown in Tab. 7. Tab. A.11 presents the results where we can see that CA calibrators perform better than CW LR. Secondly, while CA LR obtains on par performance with CA IR while combining ATSS and PAA, it performs worse once RS R-CNN is in the mixture. This is because the calibration error of CA LR is higher than CA IR (for late calibration) in terms of all calibration measures as shown in Tab. 7). This suggests that CA LR cannot mitigate the incompatibility of the detectors properly with a higher calibration error. Considering these results and calibration performance, we prefer CA IR while obtaining MoEs via our MoCaE.

B.3. Further Details and Analyses on Deep Ensembles

Obtaining DEs and the Effect of Calibration on DEs DEs combine the same models that are trained from different initializations of the parameters. Ideally, the expectation over the predictive distributions of the components in a DE yields the prediction of the DE. This can be easily obtained for classifiers which predict a categorical distribution over the classes given an input image. On the other hand, it is not straightforward to use DEs for detectors as there is no clear way to associate detections from different detectors. As a result, similar to MoCaE, we obtain DEs by using late calibration as shown in Fig. 3(a), which turns out to be an effective method. To see that, we first present the single model performance of the five different components comprising DEs in Tab. A.12. Then, from these single detectors, we obtain DEs for PAA with and without calibration using the standard NMS. Tab. A.13 shows that this way of obtaining DEs is effective as the performance increases when the number of components increases. We observe that increasing the number of components improve the performance between $0.1-0.3$ AP. On the other hand, as there is no incompatibility among different detectors in a DE, the effect of calibration is not notable for DEs.

B.4. Sensitivity of MoCaE to Design Choices in Refining NMS

As introduced in App A, Refining NMS combines Soft NMS and Score Voting. Specifically, Soft NMS can be linear or gaussian; furthermore both Soft NMS (either linear or gaussian) and Score Voting have hyper-parameters. Here, we investigate the sensitivity of MoCaE to such design choices

[2]To keep this number manageable, we use top-1000 detections predicted from each pyramid level for ATSS and PAA for early calibration.

Table A.11. Comparison of different calibration methods to obtain MoEs. CA IR performs better than other methods.

Calibrated	RS R-CNN	ATSS	PAA	AP	AP50	AP75	APS	APM	APL
N/A	✓			42.4	62.1	46.2	26.8	46.3	56.9
(Single		✓		43.1	61.5	47.1	27.8	47.5	54.2
Models)			✓	43.2	60.8	47.1	27.0	47.0	57.6
✗	✓	✓		42.4	62.1	46.3	26.8	46.3	56.9
CW LR	✓	✓		43.0	61.4	46.9	28.1	47.2	54.4
CA LR	✓	✓		43.7	62.5	47.7	28.7	48.2	55.2
CA IR	✓	✓		44.1	63.0	48.4	28.5	48.4	56.8
✗	✓		✓	43.4	62.5	47.1	27.3	47.3	58.0
CW LR	✓		✓	42.7	61.8	46.7	27.1	46.5	57.6
CA LR	✓		✓	43.5	63.0	47.7	27.9	47.5	57.8
CA IR	✓		✓	44.0	62.7	47.9	28.2	48.2	58.1
✗		✓	✓	43.3	60.9	47.2	27.1	47.2	57.6
CW LR		✓	✓	42.6	60.7	46.5	26.6	47.2	53.9
CA LR		✓	✓	44.4	62.5	48.3	29.0	48.3	57.3
CA IR		✓	✓	44.4	62.5	48.5	29.2	48.5	57.3
✗	✓	✓	✓	43.4	62.5	47.1	27.3	47.3	58.0
CW LR	✓	✓	✓	43.0	61.3	47.1	28.2	47.4	54.6
CA LR	✓	✓	✓	44.0	62.7	48.1	29.0	48.5	55.8
CA IR	✓	✓	✓	44.7	63.1	48.9	29.2	49.0	58.2

Table A.12. Single model performance of the detectors that we used in DEs. While obtaining MoEs, we combine "Model 1" of different types of detectors.

Model	AP	AP_{50}	AP_{75}	AP_S	AP_M	AP_L
RS R-CNN (Model 1)	42.4	62.1	46.2	26.8	46.3	56.9
RS R-CNN (Model 2)	42.6	62.7	46.7	27.3	46.5	55.8
RS R-CNN (Model 3)	42.6	62.6	46.5	27.2	46.8	56.1
RS R-CNN (Model 4)	42.6	62.3	46.1	27.9	46.1	55.9
RS R-CNN (Model 5)	42.2	62.8	45.8	26.7	46.5	55.7
ATSS (Model 1)	43.1	61.5	47.1	27.8	47.5	54.2
ATSS (Model 2)	43.3	61.5	47.5	28.9	47.8	55.0
ATSS (Model 3)	43.3	61.5	47.0	28.9	47.9	55.8
ATSS (Model 4)	43.0	61.2	46.8	29.0	47.4	54.6
ATSS (Model 5)	43.3	61.5	47.5	28.2	47.7	54.8
PAA (Model 1)	43.2	60.8	47.1	27.0	47.0	57.6
PAA (Model 2)	43.5	61.0	47.3	27.5	47.7	57.7
PAA (Model 3)	43.4	61.1	47.2	27.7	47.6	57.8
PAA (Model 4)	43.6	61.4	47.2	27.6	47.6	57.6
PAA (Model 5)	43.6	61.3	47.2	27.9	47.9	58.0

using Soft NMS as an example using RS R-CNN, ATSS and PAA for COCO; and the setting described in Sec. 4 for LVIS. We can easily see in Tab. A.14 that Vanilla MoE does not benefit properly from Soft NMS without calibration. For example, there is no gain for Linear Soft NMS, the performance degrades for the Gaussian Soft NMS on COCO and the gain is only 0.4 for LVIS. This is expected as a single hyper-parameter to reconciliate the scores all detectors might not be sufficient especially for the Gaussian Soft NMS. On the other hand, after calibration, we consistently see the gains for our MoCaE: MoCaE benefits slightly on COCO dataset both for linear and gaussian cases; and besides, the gain on LVIS is 1.0 mask AP. This is because, the scores are compatible for each detector after calibration and a single hyperparameter allows Soft NMS to properly adjust the scores from different detectors. We choose Linear Soft

Table A.13. The effect of increasing the components and using calibration on DEs. Increasing the components improves the performance while calibration does not have a notable effect on performance for DEs unlike their importance for MoEs.

Model	Calibration	AP	AP_{50}	AP_{75}	AP_S	AP_M	AP_L
PAA × 2	✗	43.8	61.4	47.6	28.2	48.3	58.3
	✓	43.9	61.4	47.7	28.0	48.3	58.6
PAA × 3	✗	44.1	61.5	48.0	28.8	48.7	58.8
	✓	44.1	61.6	48.0	28.7	48.7	58.9
PAA × 4	✗	44.3	61.7	48.3	28.9	48.8	59.1
	✓	44.3	61.7	48.3	28.9	48.8	59.1
PAA × 5	✗	44.4	61.7	48.6	29.1	49.0	59.3
	✓	44.4	61.7	48.6	28.9	49.0	59.3

Table A.14. Sensitivity of Vanilla MoE and MoCaE to different configurations of Soft NMS. The results are presented on COCO mini-test and 500 validation images that we used to train the calibrators for LVIS.

Method	Soft NMS	COCO (box AP)	LVIS (mask AP)
Vanilla MoE	✗	**43.4**	37.5
	Linear, $IoU_{NMS} = 0.65$	**43.4**	37.5
	Gaussian, $\sigma_{NMS} = 0.20$	41.6	**37.9**
	Gaussian, $\sigma_{NMS} = 0.40$	42.1	37.8
	Gaussian, $\sigma_{NMS} = 0.60$	42.4	**37.9**
	Gaussian, $\sigma_{NMS} = 0.80$	42.7	37.8
	Gaussian, $\sigma_{NMS} = 1.00$	42.9	37.9
MoCaE	✗	44.7	39.8
	Linear, $IoU_{NMS} = 0.65$	**44.8**	39.9
	Gaussian, $\sigma_{NMS} = 0.20$	43.7	40.6
	Gaussian, $\sigma_{NMS} = 0.40$	44.4	**40.8**
	Gaussian, $\sigma_{NMS} = 0.60$	**44.8**	40.6
	Gaussian, $\sigma_{NMS} = 0.80$	44.7	40.2
	Gaussian, $\sigma_{NMS} = 1.00$	44.6	39.9

NMS on COCO resulting in the best results for Vanilla MoE and MoCaE. For LVIS, we use Gaussian Soft NMS with $\sigma_{NMS} = 0.40$ for MoCaE. In a similar way, we validate the hyper-parameter of Score Voting as 0.04.

B.5. The contribution of MoCaE on performance aspects

We now analyse what performance aspects, among localisation, recall and precision, are affected by MoCaE by expliting three different analyses tools from the detection literature. First, we use TIDE that defines oracle APs as the APs obtained when FP and false-negative (FN) errors are completely mitigated. Then, the difference between the oracle and actual AP correspond to the error of a detector for a specific performance aspect. More specifically, while obtaining Oracle FP AP, the FP detections are simply removed from the final detection set. As for Oracle FN AP, the FN objects are removed from the dataset. Fig. A.6(a) shows that MoCaE variants perform similar to the single detectors in terms of FP Error while they clearly outperform them on FN Error. This indicates that one of the contributions of MoE is to find the objects that are not detected by at least one of the individual detector as illustrated on Fig. 1 and Tab. 1. However, TIDE analysis does not provide insight on the localisation quality which is mainly targeted by Refining NMS. Therefore, in our second analysis we exploit AR defined as the average of the recall values over 10 IoUs from 0.50 to 0.95. Aligned with the observation in TIDE analysis, Fig. A.6(b) presents that MoCaE improves AR of the single detectors. Furthermore, the performance gain mainly originates from the improvement in small and medium objects as MoCaE does not improve the performance on large objects notably. This indicates that the resulting MoE is especially stronger than single detectors in more challenging object categories. Using Refining NMS further boosts the AR performance as it improves the localisation performance, which is critical for recalls with higher IoUs. To investigate the benefit of MoE in practical use-cases, we finally conduct an

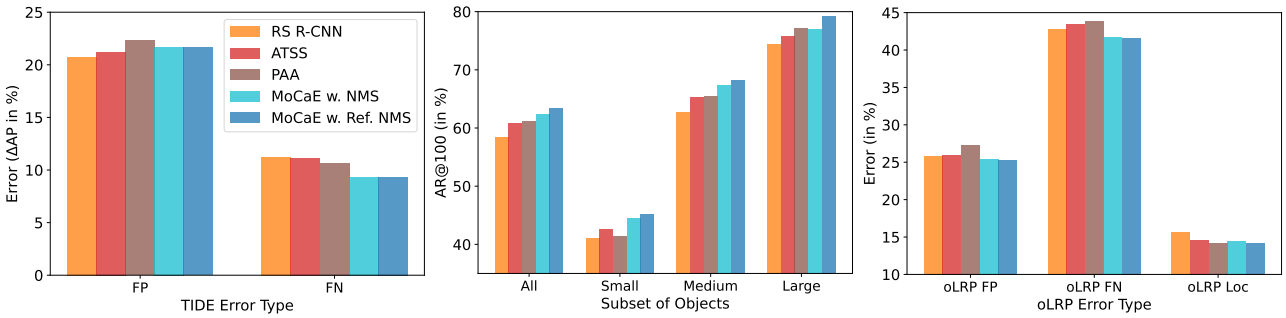

(a) TIDE-style Analysis [3] (b) Average Recall (c) LRP Error Components [53]

Figure A.6. The contribution of MoCaE on performance aspects

LRP analysis [50, 53] in Fig. A.6(c). In this figure, oLRP FP, FN and Loc correspond to the components Optimal LRP Error defined as 1-Precision, 1-Recall and the average IoU Error of TP detections. Aligned with our previous analysis, MoE mainly decreases the recall error and MoCaE with Refining NMS mainly contributes to the oLRP Loc component, outperforming all individual models in the end. These three different analyses confirm that MoCaE with NMS mainly decreases the recall error of the detector and using Refining NMS contributes to the localisation error.

B.6. Full Version of the Tables/Figures that are Pruned in the Main Paper

Tab. A.15 presents the details of the evalution on LVIS; Tab. A.16 includes the performance of all classes for DOTA dataset; and Tab. A.17 shows the exact values used to obtain Fig. 4. These tables are excluded from the main paper due to the space limitation.

Table A.15. Detailed results on LVIS val set. The detectors have different characteristics in terms of exploiting Repeat Factor Sampling (RFS), backbone, the number of training epochs and the loss function. While Vanilla MoE does not yield gain, MoCaE enables a stronger MoE than all single detectors.

Method	RFS	Backbone	Epoch	Instance Segmentation Performance						Object Detection Performance					
				AP	AP_{50}	AP_{75}	AP_r	AP_c	AP_f	AP	AP_{50}	AP_{75}	AP_r	AP_c	AP_f
Seesaw Mask R-CNN [62]	✗	ResNet-50	24	25.4	39.5	26.9	15.8	24.7	30.4	25.6	41.6	26.6	14.0	24.0	32.3
RS Mask R-CNN [52]	✓	ResNet-50	12	25.1	38.2	26.8	16.5	24.3	29.9	25.8	39.7	27.8	15.1	24.5	32.0
Mask R-CNN [22]	✓	ResNeXt-101	12	25.4	39.2	27.3	15.7	24.7	30.4	26.6	42.1	28.5	15.4	25.2	33.1
Vanilla MoE	N/A	N/A	N/A	25.2	38.3	26.8	16.5	24.3	29.9	25.9	39.8	27.9	15.1	24.5	32.2
				−0.2	−1.2	−0.5	0.0	−0.4	−0.5	−0.7	−2.3	−0.6	−0.3	−0.7	−0.9
MoCaE (Ours)	N/A	N/A	N/A	**27.7**	**42.8**	**29.4**	**18.2**	**27.3**	**32.4**	**29.1**	**44.8**	**31.4**	**17.0**	**27.9**	**35.8**
				+2.3	+3.3	+2.1	+1.7	+2.4	+2.0	+2.5	+1.6	+2.9	+1.6	+2.7	+2.7

Table A.16. The performance of all classes on DOTA v1.0. AP_{50} is reported as the performance measure of DOTA.

Detector	All	Dataset Classes													
		Plane	Baseba.	Bridge	Ground-t.	Small-veh.	Large-veh.	Ship	Tennis	Basket.	Storag.	Soccer	Roundab.	Harbor	Swimm.	Helico.
RTMDet	81.32	88.04	86.20	58.50	82.43	81.21	84.87	88.70	**90.89**	**88.75**	87.33	72.12	70.85	81.16	81.49	77.24
LSKN (prev. SOTA)	81.85	**89.69**	85.70	61.47	83.23	81.37	**86.05**	88.64	90.88	88.49	**87.40**	71.67	71.35	79.19	81.77	80.85
Vanilla MoE	80.60	87.76	83.27	**61.77**	78.25	81.26	85.33	88..34	89.93	85.54	86.35	70.98	65.92	84.28	**82.45**	77.57
	−1.25	−1.93	−2.93	+0.30	−4.98	−0.11	−0.72	−0.36	−0.11	−0.96	−1.05	−1.14	−5.43	+3.12	+0.68	−3.28
MoCaE (Ours)	**82.62**	89.09	**86.47**	61.38	**83.28**	**81.43**	85.03	**88.72**	90.86	88.31	87.11	**75.50**	**74.12**	**84.49**	81.63	**81.93**
	+0.77	−0.60	+0.27	−0.09	+0.05	+0.06	−1.02	+0.02	−0.03	−0.44	−0.29	+3.38	+2.77	+3.33	−0.14	+1.08

Table A.17. The values used in Fig. 4. The area of the dots are associated with the NMS time for the detectors given a specific background removal threshold. Early calibration regularizes the behaviour of the detectors by reducing their sensitivity to background removal threshold with respect to AP and NMS time. NMS time is measured in terms of ms using a single Nvidia 1080ti GPU.

Background Removal Threshold	Detector	Uncalibrated		Early Calibrated	
		AP	NMS time	AP	NMS time
0.05	F-RCNN	40.1	0.5	40.3	0.6
	RS-RCNN	42.4	35.4	42.4	0.6
	ATSS	43.1	0.6	43.1	0.7
	PAA	43.3	29.2	43.2	0.8
0.25	F-RCNN	38.6	0.4	39.6	0.5
	RS-RCNN	42.4	2.0	41.9	0.5
	ATSS	38.0	0.5	42.7	0.6
	PAA	43.2	1.1	42.7	0.5
0.50	F-RCNN	36.2	0.4	35.7	0.4
	RS-RCNN	42.1	0.4	38.6	0.4
	ATSS	19.3	0.4	39.3	0.5
	PAA	39.2	0.5	39.3	0.5
0.75	F-RCNN	32.1	0.4	26.5	0.4
	RS-RCNN	25.1	0.4	30.4	0.4
	ATSS	1.4	0.0	30.7	0.5
	PAA	21.0	0.4	29.6	0.5